J. Fluid Mech. (1992), *vol.* 239, *pp.* 409–427
Printed in Great Britain

Parametric resonance in low-frequency magnetic stirring

By J. M. GALPIN[1]†, Y. FAUTRELLE[1] AND A. D. SNEYD[2]

[1] INPG-MADYLAM, B.P. 95X, 38402 St Martin d'Hères Cedex, France

[2] University of Waikato, Private Bag, Hamilton, New Zealand

(Received 18 September 1990 and in revised form 19 August 1991)

This paper analyses the effect of an alternating magnetic field of low frequency ω on a cylindrical tank of liquid metal. Previous work with higher-frequency fields has focused attention on the mean recirculating motion, but in the low-frequency limit periodic motion and surface waves become important. We show that a system of forced standing axisymmetric waves of frequency 2ω is established, and that the growth of non-axisymmetric modes is governed by a coupled system of Mathieu-type equations. The stability regions associated with this system are discussed and it is shown that the most easily excited transition to a non-axisymmetric mode is subharmonic, with frequency ω. Comparison with experiment shows that the theory gives qualitatively correct predictions.

1. Introduction

When a liquid metal is placed in an alternating magnetic field, electric currents are induced which interact with the original magnetic field to create electromagnetic body forces. The consequent flow has a number of important applications in liquid-metal technology, including stirring of continuously cast steel and of the melt in induction furnaces.

The Lorentz force generally consists of two components: (i) a mean component, (ii) an oscillatory component whose frequency is twice that of the applied magnetic field. The effects of the mean component have been extensively studied by many authors (Sneyd 1971, 1979; Tarapore & Evans 1976; Mikelson, Jakovitch & Pavlov 1978; Fautrelle 1981; Moffatt 1984; Moore & Hunt 1984; Trakas, Tabeling & Chabrerie 1984; Taberlet & Fautrelle 1985; Davidson, Hunt & Moros 1988). It is generally responsible for a mean recirculating motion – the so-called electromagnetic stirring.

The oscillatory component of the Lorentz force has been largely neglected by the above authors, who were concerned with high frequencies. The first experiments in the low-frequency regime ($\omega \leqslant 10$ Hz) were performed by Galpin & Fautrelle (1992, hereinafter referred to as GF). They have shown that the oscillatory component may generate complex free-surface motions which consist of a variety of standing-wave patterns, depending on the frequency and magnetic field strength. These surface waves present some similarities with the phenomenon of parametric resonance, the best known study of which is due to Faraday (1831) who observed vibrations of a liquid contained in an oscillating vessel. He noticed free-surface oscillations whose frequency was half that of the vessel. A linear analysis of this problem has been carried out by Benjamin & Ursell (1954), who showed that in the inviscid small-amplitude case the growth of the various free-surface modes is governed by a

† Present address: IRSID, Station d'Essais, 57210 Maizières-les-Metz, France.

decoupled system of Mathieu equations, and that subharmonic instability could occur. More recently Miles (1984) has considered resonant forcing of waves in a circular cylinder by horizontal oscillations, and a general review of parametric excitation is given by Miles & Henderson (1990). Another kind of parametric instability has been discovered by Briskman & Shaidurov (1968). They showed that when a liquid free surface is subjected to a normal alternating electric field, small-amplitude free-surface displacements are governed by a Mathieu equation as in the Faraday problem. Their theory is confirmed by experiment.

The aim of this paper is to analyse some of the free-surface instabilities observed by GF. We consider a cylindrical liquid-metal pool whose axis is vertical, placed in a uniform vertical alternating magnetic field. In the low-frequency limit (a more precise criterion is given in §2) the magnetic field due to the induced currents is negligible in comparison with applied field $\boldsymbol{B}_0$. The induced currents are in quadrature (90° out of phase) with $\boldsymbol{B}_0$ and the corresponding electromagnetic forces are purely oscillatory to leading order (Taberlet & Fautrelle 1985). Furthermore, if the applied field is axial and uniform as considered in this paper, the basic electromagnetic force is both radial and irrotational. We develop a linear theory, first of axisymmetric standing waves ($m = 0$), and then find that the growth of non-axisymmetric modes ($m = 1, 2, \ldots$) is described by a system of Mathieu equations. We note two important features of the system, namely: (i) the existence of forced axisymmetric waves, (ii) the coupling of the various radial modes for a given m, which is due to the radial dependence of the basic induced electric current.

The governing equations are derived in §2. A general discussion of stability properties is given in §3, and in §4 the results are discussed and compared with experiment. Our conclusions are summarized in §5.

2. Derivation of equations

2.1. *Approximations*

We consider a uniform alternating magnetic field

$$\boldsymbol{B} = B_0 \sin(\omega t)\,\hat{\boldsymbol{z}} \tag{2.1}$$

acting on a body of conducting fluid of density ρ and electrical conductivity σ. The induced electric field drives an oscillatory electric current in the fluid, which interacts with the applied magnetic field to generate a Lorentz force having a steady component and one oscillating with angular frequency 2ω.

The MHD equations (in standard notation) are

$$\nabla \times \boldsymbol{E} = -\frac{\partial \boldsymbol{B}}{\partial t}, \tag{2.2}$$

$$\nabla \times \boldsymbol{B} = \mu_0 \boldsymbol{J}, \tag{2.3}$$

$$\boldsymbol{J} = \sigma(\boldsymbol{E} + \boldsymbol{V} \times \boldsymbol{B}), \tag{2.4}$$

$$\rho \frac{\mathrm{D}\boldsymbol{V}}{\mathrm{D}t} = -\nabla p + \boldsymbol{J} \times \boldsymbol{B}, \tag{2.5}$$

$$\nabla \cdot \boldsymbol{V} = 0, \tag{2.6}$$

where the flow is assumed inviscid and incompressible. We shall make two approximations throughout this work: first the magnetic diffusion time $L^2\mu_0\sigma$ (L a typical lengthscale) is assumed much smaller than the field-oscillation period, so

$$\omega L^2 \mu_0 \sigma / 2\pi = \epsilon \quad \text{(say)} \quad \ll 1.$$

Essentially we are assuming that the field is oscillating slowly, with $\omega \leqslant 10$ Hz for practical purposes. This assumption also means that the field due to induced currents is negligible in comparison with the applied field, and may be neglected. Second, we shall neglect the induced electric field term $\boldsymbol{V} \times \boldsymbol{B}$ in (2.4). Equations (2.2), (2.4) and (2.5) give order of magnitude estimates

$$E \approx L\omega B_0, \quad J \approx \sigma L\omega B_0, \quad v \approx \sigma L B_0^2/4\rho, \tag{2.7}$$

the factor of 4 being introduced to simplify subsequent formulae. The second assumption is therefore valid provided

$$\frac{vB_0}{E} = \frac{\sigma B_0^2}{4\omega\rho} = S \ll 1,$$

where S is the magnetic interaction parameter. This means essentially that the magnetic field must not be too intense. Taking $L = 10^{-1}$ m, $\mu_0 = 4\pi \times 10^{-7}\ \Omega$ s m^{-1}, $\sigma = 10^6\ \Omega^{-1}$ m^{-1}, $B_0 = 10^{-1}$ T, as in the experiments of GF we find for the frequency range $1 < \omega < 10$ Hz,

$$10^{-2} < \epsilon < 10^{-1}, \quad 0.04 > S > 0.004,$$

so the assumptions seem reasonable.

If we introduce non-dimensional variables

$$\boldsymbol{B} = B_0 \boldsymbol{B}', \quad \boldsymbol{J} = \sigma\omega a B_0 \boldsymbol{J}', \quad \frac{\partial}{\partial t} = \omega \frac{\partial}{\partial t'},$$

then (2.2) and (2.3) can be written in the form

$$\nabla \times \boldsymbol{J}' = -\frac{\partial \boldsymbol{B}'}{\partial t'}, \tag{2.8}$$

$$\nabla \times \boldsymbol{B}' = \epsilon \boldsymbol{J}'. \tag{2.9}$$

To zeroth order, (2.9) gives $\nabla \times \boldsymbol{B} = 0$, so we can write

$$\boldsymbol{B} = B_0[\sin(\omega t)\,\hat{\boldsymbol{z}} + O(\epsilon)].$$

Thus we may neglect the magnetic field due to the induced electric current $\boldsymbol{J}$, which is responsible for the mean component of the Lorentz force. From (2.8) we see that $\boldsymbol{B}$ and $\boldsymbol{J}$ are 90° out of phase, so to leading order the Lorentz force is purely oscillatory with frequency 2ω. The presence of slight damping, such as viscosity, ensures that the ensuing fluid motion too will eventually become purely periodic with frequency 2ω (provided of course that the forcing frequency is not close to a resonance of the system).

2.2. *Axisymmetric modes in a cylindrical tank*

Experiments were performed in a cylindrical tank, so this is the geometry we consider in detail – a body of liquid metal bounded by rigid non-conducting walls $r = a$, $-h \leqslant z \leqslant 0$, a rigid base $z = -h$, $0 \leqslant r \leqslant a$, and a free surface $z = \eta$.

The induced electric field is azimuthal: $\boldsymbol{E} = E(r,t)\,\hat{\boldsymbol{\theta}}$, and substitution into (2.2) yields

$$r^{-1}\partial/\partial r\,(rE) = -\omega B_0 \cos(\omega t), \quad \text{so} \quad E = -\tfrac{1}{2}\omega B_0\, r \cos(\omega t).$$

The induced current is therefore

$$\boldsymbol{J} = -J_{\mathrm{I}}(r/a)\cos(\omega t)\,\hat{\boldsymbol{\theta}}, \quad J_{\mathrm{I}} = \tfrac{1}{2}\sigma\omega B_0 a,$$

and the Lorentz force,

$$\boldsymbol{F} = -F_0\,(r/a)\sin(2\omega t)\,\hat{\boldsymbol{r}}, \quad F_0 = \tfrac{1}{2}J_{\mathrm{I}}B_0.$$

The fluid velocity estimate (2.7) shows that the ratio of the convective to time derivatives in $\mathrm{D}\boldsymbol{V}/\mathrm{D}t$ is of order S (which has already been assumed small), so (2.5) is approximated by

$$\rho\frac{\partial \boldsymbol{V}}{\partial t} = -\nabla p + \boldsymbol{F}. \tag{2.10}$$

Taking divergences and assuming incompressibility yields

$$\nabla^2 p = \nabla\cdot\boldsymbol{F} = \frac{-2F_0}{a}\sin(2\omega t). \tag{2.11}$$

Equation (2.10) and the usual linearized kinematic condition at the free surface, imply

$$\left(\frac{\partial p}{\partial z}\right)_{z=0} = -\rho(\dot{u}_z)_{z=0} = -\rho\ddot{\eta}, \tag{2.12}$$

while zero normal flow at the walls gives

$$\left(\frac{\partial p}{\partial r}\right)_{r=a} = -F_0\sin(2\omega t), \quad \left(\frac{\partial p}{\partial z}\right)_{z=-h} = 0. \tag{2.13}$$

A particular solution of (2.11) and (2.13) is

$$p = \frac{-F_0 r^2}{2a}\sin(2\omega t).$$

To obtain the general solution we expand the free-surface displacement in the form

$$\eta = \sum_{n=1}^{\infty} A_n(t)\,J_0(l_n r), \tag{2.14}$$

where $J_0(x)$ is a Bessel function, and l_n the nth zero of $J_0'(la)$. Note that since

$$\int_0^a rJ_0(l_n r)\,\mathrm{d}r = 0,$$

the mean free-surface displacement is zero. Using the kinematic free-surface condition (2.12) we can now write

$$p = p_0 - \frac{F_0 r^2}{2a}\sin(2\omega t) - \rho\sum_{n=1}^{\infty}\ddot{A}_n J_0(l_n r)\frac{\cosh[l_n(z+h)]}{l_n\sinh(l_n h)}, \tag{2.15}$$

where p_0 is a function of time only. At the free surface, the total pressure is zero, so to first order in η,

$$(p)_{z=0} + \frac{\partial P}{\partial z}\eta = 0,$$

where $P = -\rho g z$ is the unperturbed pressure. Since the mean value of η is zero so must be the mean value of $(p)_{z=0}$, whence from (2.15) $p_0 = \frac{1}{4}F_0 a\sin(2\omega t)$. Substituting for η and p from (2.14) and (2.15) one finds

$$\frac{F_0}{4a}(a^2 - 2r^2)\sin(2\omega t) - \rho\sum_{n=1}^{\infty}\frac{\ddot{A}_n}{\tanh(l_n h)\,l_n}J_0(l_n r) = \rho g\sum_{n=1}^{\infty}A_n J_0(l_n r). \tag{2.16}$$

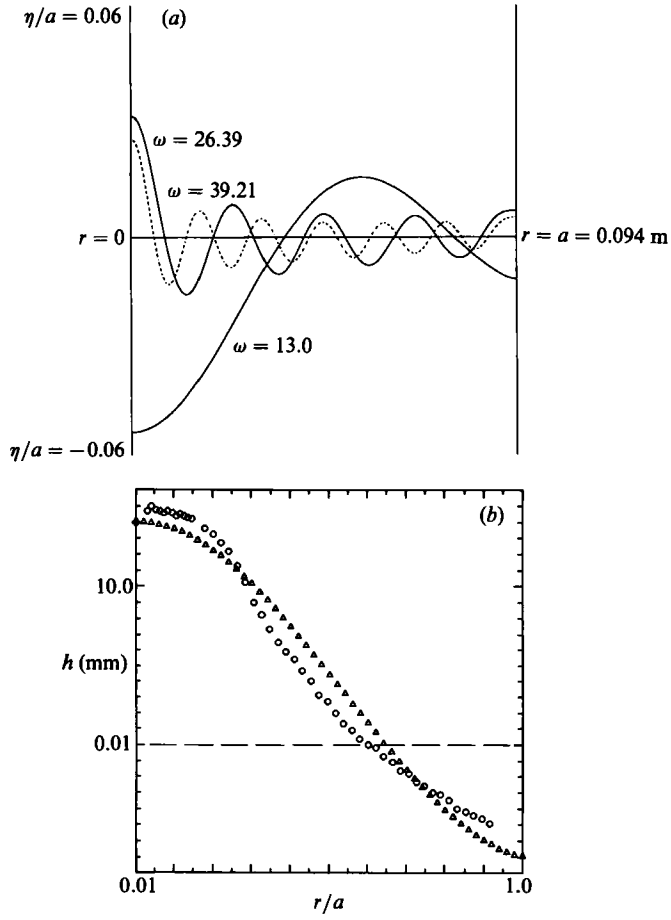

FIGURE 1. (*a*) Free-surface profiles for forced axisymmetric waves, as given by equation (2.18). The results are for a tank of mercury of radius 94 mm and depth 124 mm (as used by GF) and an applied field strength 0.1 T. All quoted frequencies are in rad s^{-1}. Note that the first six natural frequencies are 19.89, 26.91, 32.41, 37.09, 41.24, 45.01. (*b*) Theoretical (△) and experimentally measured (○) free-surface profile for $\omega = 9.39$ and a current of 82.5 A.

Multiplying (2.16) by $rJ_0(l_k r)$, integrating from $r = 0$ to $r = a$, and using the identities

$$\frac{\mathrm{d}}{\mathrm{d}x}(x^n J_n(x)) = x^n J_{n-1}(x), \quad J_2(x) = -2x^{-1}J_0'(x) - J_0(x),$$

we obtain the following differential equation for A_k:

$$\ddot{A}_k + \tanh(l_k h)\, l_k g A_k = c_k \sin(2\omega t), \quad c_k = \frac{-2F_0 \tanh(l_k h)}{\rho l_k a J_0(l_k a)}. \tag{2.17}$$

Since we are concerned only with the eventual quasi-steady state, in which the fluid motion is purely periodic with angular frequency 2ω, we may assume A_k proportional to $\sin(2\omega t)$. Substituting the appropriate solution of (2.17) into (2.16) we obtain

$$\eta = \tfrac{1}{2} a S \sin(2\omega t) \sum_{n=1}^{\infty} \frac{\omega_g^2 J_0(l_n r) \tanh^2(l_n h)}{J_0(l_n a)\, \omega_n^2 (1 - \omega_n^2/4\omega^2)}, \tag{2.18}$$

where $\omega_g = (g/a)^{\frac{1}{2}}$ is a gravitational frequency, $\omega_n^2 = \tanh(l_n h)\, l_n g$ represents the nth

2ω	18.79	25.51	50.90
Nearest ω_n	19.89	26.92	51.72
η_0 (experimental)	4.2	3.4	2.6
η_0 (theoretical)	4.2	3.4	2.5

TABLE 1. Comparison of experimental and theoretical free-surface elevations η_0 at the centre of the tank. In each case the current in coils was 45.0 A, giving $B_0 = 0.1$ T. All length measurements are quoted in mm.

resonant frequency, and $S = \sigma B_0^2/4\rho\omega$ is the interaction parameter. Since we have assumed $S \ll 1$, the free-surface displacements will be small compared with the cylinder radius, except when ω is close to one of the natural frequencies ω_n. In this case our linearized analysis leading to (2.18) is invalidated by the large displacements. Physically these large displacements are limited by nonlinear effects and dissipation (e.g. viscosity).

Figure 1(*a*) shows free-surface profiles calculated from (2.18) for various frequencies used in the GF experiments. Note that both the amplitude and wavelength decrease as ω increases. It is clear from (2.18) that the dominant mode will be that whose natural frequency ω_n is nearest to 2ω. Figure 1(*b*) compares a theoretical and an experimentally measured free-surface profile, and table 1 lists observed and theoretical maximum amplitudes η_0 at the centre of the tank, for various ω.

2.3. *Growth of non-axisymmetric perturbations*

2.3.1. *Current perturbation*

In the axisymmetric state the purely azimuthal electric current $\boldsymbol{J}$ is unperturbed since it flows parallel to the free-surface contours. However when η depends upon θ, the current flow must be modified to follow the contours of the free surface and satisfy the boundary condition $\boldsymbol{J}\cdot\hat{\boldsymbol{n}} = 0$.

We now consider a free-surface perturbation of the form

$$\eta_m = a\,\mathrm{e}^{\mathrm{i}m\theta}\sum_{n=1}^{\infty}\alpha_n(t)\,\phi_n(r), \quad \phi_n(r) = \frac{J_m(\lambda_n r)}{J_m(\lambda_n a)},$$

where m is a positive integer and λ_n the nth zero of $J'_m(\lambda a)$.

Let $\boldsymbol{j}_m$ be the electric current perturbation, $\boldsymbol{b}_m$ the magnetic field due to $\boldsymbol{j}_m$, and $\boldsymbol{v}_m$ the corresponding flow perturbation. (We shall generally use the subscript m to label the $\mathrm{e}^{\mathrm{i}m\theta}$ variation in any variable.) If h_m is a typical magnitude of η_m, then the condition that $\boldsymbol{j}_m$ be parallel to the free-surface implies $|\boldsymbol{j}_m| = O(mh_m J_\mathrm{I}/a)$. For simplicity we shall consider only the larger m modes – say $m \geqslant 5$. Indeed in the GF experiments many of the observed modes corresponded to larger values of m, specifically $m = 5$, 8, 12, 23. Now consider the $\mathrm{e}^{\mathrm{i}m\theta}$ component of (2.4),

$$\boldsymbol{j}_m = \sigma(\boldsymbol{E}_m + \boldsymbol{v}_m \times \boldsymbol{B} + \boldsymbol{v}_0 \times \boldsymbol{b}_m).$$

On the right-hand side the last two 'induction' terms are smaller than the first 'geometrical' term by a factor m^{-1}, and can be neglected.

To leading order (2.9) gives $\nabla \times \boldsymbol{b}_m = 0$, and hence $\boldsymbol{b}_m = 0$. Using the above large-m approximation we find

$$\nabla \times \boldsymbol{j}_m = \sigma \nabla \times \boldsymbol{E}_m = -\sigma \frac{\partial \boldsymbol{b}_m}{\partial t} = 0,$$

so we can write $\boldsymbol{j}_m = \nabla V$ say. To leading order in h_m the unit normal vector to the free surface is $\hat{\boldsymbol{z}} - \nabla\eta_m$ and the condition of zero normal current flow implies

$$\left(\boldsymbol{j}_m - \frac{J_I r}{a}\hat{\boldsymbol{\theta}}\right)\cdot(\hat{\boldsymbol{z}} - \nabla\eta_m) = 0.$$

To leading order in h_m, this gives

$$\left(\frac{\partial V}{\partial z}\right)_{z=0} = -\frac{imJ_I}{a}\cos(\omega t)\,\eta_m.$$

Since $\nabla\cdot\boldsymbol{j}_m = 0$ and no current flows across any boundary, v must also satisfy

$$\nabla^2 V = 0, \quad \left(\frac{\partial V}{\partial r}\right)_{r=0,a} = 0, \quad \left(\frac{\partial V}{\partial z}\right)_{z=-h} = 0.$$

Introducing the harmonic functions

$$Q_n(r,\theta,z) = e^{im\theta}\phi_n(r)\,Z_n(z), \quad Z_n(z) = \frac{\cosh[\lambda_n(z+h)]}{\lambda_n a \sinh(\lambda_n h)}, \tag{2.19}$$

we can write the solution for V as

$$V = -imJ_I a\cos(\omega t)\sum_{n=1}^{\infty}\alpha_n(t)\,Q_n.$$

2.3.2. *Pressure perturbation*

The body force $\boldsymbol{f}_m = \nabla V \times B_0 \sin(\omega t)\,\hat{\boldsymbol{z}}$ due to the surface perturbation η_m satisfies the following conditions:

$$\nabla\cdot\boldsymbol{f}_m = 0, \quad f_{mz} = \boldsymbol{f}_m\cdot\hat{\boldsymbol{z}} = 0, \quad f_{mr} = \boldsymbol{f}_m\cdot\hat{\boldsymbol{r}} = \frac{F_0 m^2 a}{r}\sin(2\omega t)\,\alpha_i(t)\,Q_i,$$

where for compact notation we use the convention that repeated suffixes i or j only are summed from 1 to infinity.

The linearized $e^{im\theta}$-component of the equation of motion is

$$\rho\left(\frac{\partial \boldsymbol{v}_m}{\partial t} + (\boldsymbol{v}_0\cdot\nabla)\,\boldsymbol{v}_m + (\boldsymbol{v}_m\cdot\nabla)\,\boldsymbol{v}_0\right) = -\nabla p_m + \boldsymbol{f}_m,$$

where $\boldsymbol{v}_0$ is the axisymmetric velocity field associated with the forced free-surface displacement (2.18). An order of magnitude analysis shows that

$$\frac{|\boldsymbol{f}_m|}{|(\boldsymbol{v}_0\cdot\nabla)\,\boldsymbol{v}_m|} \approx \frac{|\boldsymbol{f}_m|}{|(\boldsymbol{v}_m\cdot\nabla)\,\boldsymbol{v}_0|} \approx m,$$

and using again our large-m approximation we neglect forcing due to the nonlinear terms. (Although these terms are $O(S)$ compared with $\partial\boldsymbol{v}_m/\partial t$, their role in the equation of motion is that of weak parametric forcing, similar to that of $\boldsymbol{f}_k$. It is with this latter term therefore that they should be compared.) We can thus approximate the equation of motion by

$$\rho\frac{\partial \boldsymbol{v}_m}{\partial t} = -\nabla p_m + \boldsymbol{f}_m. \tag{2.20}$$

The pressure perturbation p_m therefore satisfies the following:

$$\nabla^2 p_m = 0, \quad \left(\frac{\partial p_m}{\partial z}\right)_{z=-h} = 0, \quad \left(\frac{\partial p_m}{\partial r}\right)_{r=a} = F_0 m^2 \sin(2\omega t)\, e^{im\theta}\alpha_i Z_i. \quad (2.21\,a\text{–}c)$$

The kinematic condition at the free surface is

$$\frac{\partial \eta}{\partial t} + (\boldsymbol{v})_{z=\eta_0+\eta_m} \cdot \nabla \eta = (w)_{z=\eta_0+\eta_m},$$

and the $e^{im\theta}$-component is

$$\frac{\partial \eta_m}{\partial t} + (\boldsymbol{v}_0 \cdot \nabla)\eta_m + (\boldsymbol{v}_m \cdot \nabla)\eta_0 + \left(\eta_m \frac{\partial \boldsymbol{v}_0}{\partial z} \cdot \nabla\right)\eta_0 = w_m + \frac{\partial w_0}{\partial z}\eta_m.$$

To leading order in the magnetic interaction parameter S this gives

$$\frac{\partial \eta_m}{\partial t} = (w_m)_{z=0},$$

which together with the z-component of (2.20) yields the boundary condition

$$\left(\frac{\partial p_m}{\partial z}\right)_{z=0} = -\rho \ddot{\eta}_m = -\rho a\, e^{im\theta}\ddot{\alpha}_i \phi_i. \quad (2.22)$$

The solution for p_m is found by writing $p_m = p_A + p_B$; p_A satisfies (2.21 a, b) and (2.22) and has vanishing radial derivative on $r = a$; p_B satisfies (2.21 a–c) and has a vanishing z-derivative on $z = 0$. The obvious solution for p_A is

$$p_A = -\rho a^2 \ddot{\alpha}_i Q_i.$$

To find p_B we expand Z_n as a Fourier series in the form

$$Z_n(z) = \gamma_{nj}^{(1)} \cos\left(\frac{j\pi z}{h}\right), \quad (2.23)$$

where now the repeated j is summed from 0 to ∞ and the coefficients $\gamma_{nj}^{(1)}$ are given in the Appendix. Now the boundary condition (2.21 c) can be written in the form

$$\left(\frac{\partial p_m}{\partial r}\right)_{r=a} = F_0 m^2 \sin(2\omega t)\, e^{im\theta}\alpha_i \gamma_{ij}^{(1)} \cos\left(\frac{j\pi z}{h}\right).$$

We introduce the harmonic functions R_p defined by

$$R_p(r, \theta, z) = e^{im\theta}\psi_p(r) \cos\left(\frac{p\pi z}{h}\right),$$

where
$$\psi_p(r) = \frac{hI_m(p\pi r/h)}{p\pi a I'_m(p\pi a/h)} \quad (p > 0), \qquad \psi_0(r) = \frac{r^m}{ma^m}, \quad (2.24)$$

and I_m is a modified Bessel function. Since the R_p satisfy

$$\left(\frac{\partial R_p}{\partial z}\right)_{z=0,-h} = 0, \quad \left(\frac{\partial R_p}{\partial r}\right)_{r=a} = \frac{1}{a} e^{im\theta} \cos\left(\frac{p\pi z}{h}\right)$$

it follows from (2.21 c) and (2.23) that the solution for p_B is

$$p_B = F_0 m^2 a \sin(2\omega t)\, \alpha_i \gamma_{ij}^{(1)} R_j,$$

so with (2.22) we find

$$p = F_0 m^2 \sin(2\omega t)\,\alpha_i \gamma_{ij}^{(1)} R_j - \rho a^2 \ddot{\alpha}_i(t)\, Q_i. \tag{2.25}$$

2.3.3. *System of equations*

At the free surface $z = 0$ the total pressure must vanish:

$$(p_0 + p_m)_{z=\eta_0+\eta_m} = \rho g \eta,$$

and taking $e^{im\theta}$ components gives

$$\left(\frac{\partial p_0}{\partial z}\right)_{z=0} \eta_m + (p_m)_{z=0} - \rho g \eta_m = 0.$$

The first term is $O(S)$ compared with the other two and can be neglected, so substituting for p from (2.25) yields

$$F_0 m^2 a \sin(2\omega t)\,\alpha_i \gamma_{ij}^{(1)} \psi_j(r) - \frac{\rho a \ddot{\alpha}_i(t)\,\phi_i(r)}{\lambda_i \tanh(\lambda_i h)} = \rho g a \alpha_i(t)\,\phi_i(r). \tag{2.26}$$

Now multiplying this equation by $r\phi_q(r)$ and integrating from $r = 0$ to $r = a$ we obtain

$$F_0 m^2 a \sin(2\omega t)\,\alpha_i \gamma_{ij}^{(1)} \gamma_{jq}^{(2)} - \frac{\rho a \ddot{\alpha}_q}{\lambda_q \tanh(\lambda_q h)} = \rho g a \alpha_q(t), \tag{2.27}$$

where the coefficients $\gamma_{pq}^{(2)}$ are defined in the Appendix. Finally, the system can be written in the form

$$\ddot{\alpha}_n + \Omega_n^2[\alpha_n - L_0 \sin(2\omega t)\, C_{ni}\alpha_i] = 0, \quad C_{nk} = m^2 \gamma_{kj}^{(1)} \gamma_{jn}^{(2)}, \tag{2.28a, b}$$

where $L_0 = F_0/\rho g$ is a dimensionless number measuring the ratio of magnetic to gravitational forces, and $\Omega_n^2 = g\lambda_n \tanh(\lambda_n h)$ are natural frequencies of the mth mode. Explicit formulae (A 6a, b) are given for the coefficients C_{nk} in the Appendix.

Equations (2.28a) are a generalization of the simple Mathieu equation

$$\ddot{x} + g/l\,[1 + L\cos(\omega t)]\,x = 0,$$

which describes the motion of a simple pendulum of length l whose upper support point oscillates vertically with amplitude L and frequency ω. In the case of the Mathieu equation it is possible to divide the (ω, L)-plane into regions of instability and stability, where solutions respectively grow or decay, and one would expect there to be a similar stability boundary for the system (2.28a). If the parameters are such that (ω, L_0) lies in the unstable region, then non-axisymmetric disturbances with azimuthal mode number m will grow – in other words there will be a symmetry breaking. The dominant mode m will be that with the largest growth rate.

3. General remarks on stability

Equations (2.28a) are linear, with coefficients which are periodic functions of time. The stability of such systems is investigated by calculating the *period advance mapping* g_T (see e.g. Arnol'd 1973) which advances the solution in time by one period $T = \pi/\omega$. Thus if $\boldsymbol{X}(t)$ is the vector of unknown functions and their first derivatives, i.e.

$$X_1(t) = \alpha_1(t), \quad X_2(t) = \dot{\alpha}_1(t), \quad X_3(t) = \alpha_2(t), \ldots,$$

one can write

$$\boldsymbol{X}(t+T) = g_T\, \boldsymbol{X}(t).$$

When the system is truncated to say N unknown functions, g_T is represented by a constant $2N \times 2N$ matrix, $\boldsymbol{G}_T$ say, which may be computed numerically. If $\boldsymbol{G}_T$ has an eigenvalue with absolute value greater than one, $\boldsymbol{G}_T^n$ will be unbounded as $n \to \infty$ and the system will be unstable. Conversely if all eigenvalues are less than one in absolute value the system will be stable.

Were the coefficient matrix $\boldsymbol{C}$ symmetric, (2.28a) could be written as a Hamiltonian system, and the theory of Gel'fand & Lidskii (1958) could greatly simplify the task of determining stability boundaries. Unfortunately $\boldsymbol{C}$ is not symmetric (see (A 6)) but several useful properties of Hamiltonian systems nonetheless remain valid. If (2.28a) is written as the first-order system

$$\dot{\boldsymbol{X}} = \boldsymbol{V}(\boldsymbol{X}) \tag{3.1}$$

then it is easily verified that $\nabla \cdot \boldsymbol{V} = \partial V_i / \partial X_i = 0$, and that volume is conserved in phase space (cf. Liouville's theorem for a Hamiltonian system). Thus the matrix $\boldsymbol{G}_T$ preserves volume, so we can write

$$\det(\boldsymbol{G}_T) = \prod_{i=1}^{2N} \lambda_i = 1, \tag{3.2}$$

where the λ_i are the eigenvalues of $\boldsymbol{G}_T$. The identity $\sin(2\omega t) = \sin[2\omega(t_0 - t)]$, where $t_0 = \pi/2\omega$, implies that if $\boldsymbol{X}(t)$ is a solution of (3.1), then so is $\boldsymbol{X}(t_0 - t)$. Also, it can be shown (see e.g. Jordan & Smith 1987, p. 248) that if λ is an eigenvalue of $\boldsymbol{G}_T$ then the system has a solution $\boldsymbol{X}(t)$ such that

$$\boldsymbol{X}(t+T) = \lambda \boldsymbol{X}(t).$$

If we write the solution $\boldsymbol{X}(t_0 - t)$ as $\bar{\boldsymbol{X}}(t)$ say, then

$$\bar{\boldsymbol{X}}(t+T) = 1/\lambda\, \bar{\boldsymbol{X}}(t),$$

so λ^{-1} must also be an eigenvalue. Thus the eigenvalues of $\boldsymbol{G}_T$ occur in reciprocal pairs, i.e. it is a *reciprocal matrix* as defined by Gel'fand & Lidskii (1958). Moreover since $\boldsymbol{G}_T$ is real, eigenvalues must occur in complex-conjugate pairs, and hence in quadruples of the form

$$r\mathrm{e}^{\mathrm{i}\theta}, \quad r\mathrm{e}^{-\mathrm{i}\theta}, \quad 1/r\mathrm{e}^{\mathrm{i}\theta}, \quad 1/r\mathrm{e}^{-\mathrm{i}\theta}. \tag{3.3}$$

When the eigenvalue is real, or lies on the unit circle this quadruple degenerates to a pair.

When the system is stable, (3.2) shows that each λ_i lies on the unit circle. Transition to instability can occur either (i) when two eigenvalues 'collide' at ± 1 and move off in different directions along the real axis; or (ii) when two pairs collide simultaneously at $\mathrm{e}^{\pm \mathrm{i}\theta}$ and move off radially, two inwards and two outwards from the unit circle (figure 2). We shall refer to these as type I and type II transitions respectively.

3.1. *Resonance points on the axis $L_0 = 0$*

From a practical point of view the important transitions are those which take place in the vicinity of the axis $L_0 = 0$. Such instabilities, triggered by weak threshold magnetic fields, will be most easily observed. When $L_0 = 0$ the system (2.28a) degenerates to N uncoupled simple harmonic oscillators, and it is easily shown that the matrix $\boldsymbol{G}_T$ is block diagonal, of the form

$$\boldsymbol{G}_T = \mathrm{diag}(\boldsymbol{B}_1, \boldsymbol{B}_2, \ldots, \boldsymbol{B}_n), \quad \boldsymbol{B}_i = \begin{pmatrix} \cos(\Omega_i T) & 1/\Omega_i \sin(\Omega_i T) \\ \Omega_i \sin(\Omega_i T) & \cos(\Omega_i T) \end{pmatrix}.$$

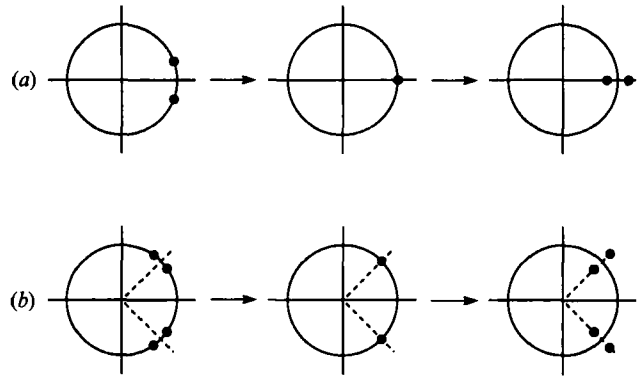

FIGURE 2. Eigenvalues in the complex plane (*a*) during a type I and (*b*) during a type II transition. The leftmost diagram is just before, and the rightmost just after the onset of instability. Eigenvalue positions are represented by black dots, and the circle shown is the unit circle.

The eigenvalues of $\boldsymbol{G}_T$ are thus $e^{\pm i\Omega_i T}$, $i = 1, 2, \ldots, N$, and a type I transition will occur when $\Omega_i T = \Omega_i \pi/\omega = k\pi$ where k is a positive integer. Thus type I transitions occur at frequencies given by

$$\omega = \Omega_i/k, \quad i = 1, 2, \ldots, N, \quad k = 1, 2, 3, \ldots. \tag{3.4}$$

Type II transitions will occur when $\Omega_i T = \pm\Omega_j T + 2k\pi$, i.e. when

$$\omega = \frac{\Omega_i + \Omega_j}{2k}, \quad \omega = \frac{\Omega_i - \Omega_j}{2k}, \tag{3.5a, b}$$

where i and j range from 1 to N, and k is a positive integer.

The frequencies (3.4) and (3.5), which we call resonance points, represent only *potential* transitions to instability – it may turn out that when L_0 increases slightly from zero, the pair (or pairs) of eigenvalues which have collided will continue around the unit circle in the complex plane, rather than branching inside and outside. The question as to whether instability occurs or not can be decided by calculating asymptotic expansions of the solutions of (2.28*a*) for small L_0. The results of Nayfeh & Mook (1979) show that unstable transitions for small positive L_0 always occur at resonance points (3.4) when $k = 1$. The asymptotic expansion of the unstable eigenvalue in the vicinity of this resonance is

$$\lambda = -1 - \tfrac{1}{4}\pi|C_{ii}|L_0 + O(L_0^2), \tag{3.6}$$

so this is called a *strong* transition in the sense that the eigenvalue moves a distance of $O(L_0)$ outside the unit circle.

For $k = 1$, in the neighbourhood of the type II resonances (3.5*a*) one finds (Nayfeh & Mook 1979)

$$\lambda = e^{i\Omega_i T}\left[1 + \frac{\pi L_0 (C_{ij} C_{ji} \Omega_i \Omega_j)^{\frac{1}{2}}}{2(\Omega_i + \Omega_j)}\right]. \tag{3.7}$$

Thus the resonances (3.5*a*) with $k = 1$ again represent a strong transition since C_{ij} and C_{ji} have the same sign. Similarly, the asymptotic expansion in the vicinity of a (3.5*b*) resonance is

$$\lambda = e^{i\Omega_i T}\left[1 + \frac{\pi L_0 (-C_{ij} C_{ji} \Omega_i \Omega_j)^{\frac{1}{2}}}{2(\Omega_i + \Omega_j)}\right],$$

and no transition occurs since the coefficient of L_0 is purely imaginary.

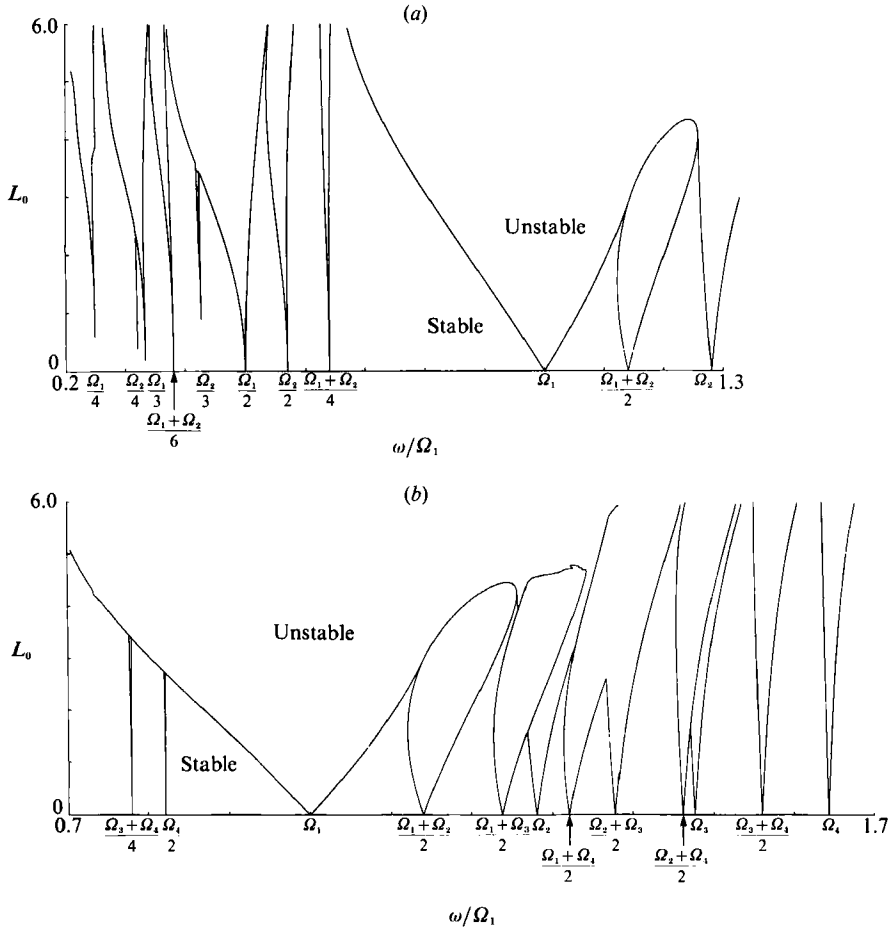

FIGURE 3. Stability regions in the (ω, L_0)-plane for $m = 5$. (*a*) $m = 5$, $N = 2$; (*b*) $m = 5$, $N = 4$. (N is the Fourier–Bessel series truncation level.)

It can be shown (Nayfeh & Mook 1979) that the resonance points (3.4) with $k = 2$ also represent type I transitions to instability, but these are *weak* in the sense that the eigenvalue moves only a distance $O(L_0^2)$ outside the unit circle, giving correspondingly small growth rates. Weak transition to instability at the type II resonance points also occurs for $k = 2$.

The higher resonances $k \geqslant 3$ have not yet been fully analysed. At a type I resonance point any growth rate must be of order L_0^3 or weaker (Nayfeh & Mook 1979) and it seems likely that our system behaves like a simple Mathieu equation, having instability regions of width $O(L_0^k)$ with growth rates also $O(L_0^k)$. A careful numerical search fails to detect instability in the immediate vicinity of these resonance points. Nevertheless, they appear to attract 'tongues' of instability, which eventually become so weak and narrow that the thread-like link to the L_0-axis is undetectable.

Figure 3 shows computed stability boundaries for $m = 5$ with the infinite series truncated to $N = 2$ or 4. (The behaviour for other m is qualitatively similar.) To determine stability at a given point (ω, ϵ) the system of differential equations was solved numerically with an RK8 routine to calculate the time-advance matrix $\boldsymbol{G}$, whose eigenvalues were then determined by means of the NAG routine F02AFF. The

stability boundary was then traced using a contour-following routine. As predicted, the boundary descends to the $L_0 = 0$ axis at the points of unstable resonance where $k = 1$ or 2, and the attracting influence of the $k \geqslant 3$ points is evident. The instability region is dominated by the strong (3.4) resonance for $k = 1$ and $i = 1$, because C_{11} is always by far the largest diagonal element. Equation (3.6) shows therefore that the largest growth rates occur at this resonance.

Although the level of truncation $N = 4$ is small it should be enough to include most physically observable transitions. As N increases new resonances are introduced, but the coefficient C_{NN} decreases approximately as N^{-2} (see (A 6*b*)) so the associated parametric instabilities become progressively weaker. Moreover since Ω_N increases approximately as $N^{\frac{1}{2}}$, the introduction of higher natural frequencies gives rise only to large-k resonance points in the vicinity of a given field frequency ω (see (3.4), (3.5)). For $k \geqslant 3$ the associated instabilities are extremely weak, and in practice will be damped by viscosity or surface tension.

3.2. *Spectrum of solutions*

Floquet theory shows that if λ is an eigenvalue of $\boldsymbol{G}_T$, then there exists a solution of the form

$$\boldsymbol{X}(t) = \lambda^{t/T}\boldsymbol{P}(t),$$

where $\boldsymbol{P}(t)$ is periodic with period T. Now $\boldsymbol{P}(t)$ will have a Fourier series expansion in terms of $e^{2in\omega t}$, with n ranging over the integers. Thus if $\lambda = \rho e^{i\theta}$ where ρ and θ are real, a typical term in the expansion of $\boldsymbol{X}(t)$ is

$$c\rho^{t/T} e^{i\omega t(2n+\theta/\pi)},$$

where c is a constant. For the strong transitions (3.4) with $k = 1$, $\theta = \pm\pi$ and the frequencies $(2n \pm 1)\,\omega$ will appear in the spectrum. We argued above that this strong transition is the most likely to be observed, so we would expect the ensuing subharmonics to dominate the spectrum. The weaker $k = 2$ transitions correspond to $\theta = 0$ and will generate no new frequencies.

In the case of the (3.5*a*) $k = 1$ transitions, $\theta = \pm\Omega_i\pi/\omega$, and we would expect to observe frequencies

$$2n\omega \pm \Omega_i,$$

which are not rational multiples of the fundamental 2ω.

4. Discussion

In this section we compare our theory with the experimental results of GF bearing in mind that the analysis is idealized, assuming a uniform applied magnetic field, and very small shield parameter (ϵ).

4.1. *Forced axisymmetric waves*

The forced standing waves are described by (2.18). It can be seen that the dominant mode n is the one whose eigenfrequency is closest to twice the applied field frequency. Provided the aspect ratio of the tank is of order unity so will be the term $\tanh(l_n h)$ in (2.18), and the wavelength L and amplitude η of the standing waves will be given by

$$L \approx g\omega_n^{-2} \approx g\omega^{-2}, \quad \eta = O(\omega^{-3}).$$

This behaviour is consistent with the experimental observations. Standing waves are no longer observable when the applied field frequency is greater than approximately 10 Hz (see figure 1).

Table 1 shows good agreement between theoretical and experimental wave heights at the centre of the tank for three different frequencies, and figure 1 shows similar agreement for a wave profile. We can be confident that the essential physics of the standing waves has been accurately modelled.

4.2. *Parametric instability of non-axisymmetric modes*

Our theory predicts that non-axisymmetric modes ($m \geqslant 1$) will grow for certain ranges of the parameters ω and L_0 representing applied frequency and (dimensionless) magnetic field strength. The strongest instability is subharmonic. This transition has indeed been observed by GF, and generally dominates the observed spectra.

A detailed quantitative comparison with the experiments is difficult. The first difficulty arises in the determination of the theoretical stability boundary in the (ω, L_0)-plane. The accurate computation of that boundary may be obtained in principle by a high level of truncation N, but it is not clear whether the form of the boundary converges as $N \to \infty$. As N increases, additional resonances Ω_N/k, etc. are introduced, and new 'tongues' of instability descend towards the $L_0 = 0$ axis. However, for a resonance point Ω_N/k to stay near a given applied frequency ω, k must increase with N (approximately as $N^{\frac{1}{2}}$). The analysis of Nayfeh & Mook (1979) indicates that parametric instability in the vicinity of Ω_N/k becomes progressively weaker with increasing k, the growth rates and tongue widths being of order L_0^k. Thus any new resonance points introduced near a given ω for larger N become progressively weaker as N increases, and are likely to disappear when any form of damping is taken into consideration. Thus for practical purpose a modest truncation should suffice and indeed all experimentally observed transitions occurred close the strongest transition Ω_1.

A second difficulty concerns the effects of viscosity and surface tension. The former will have a smoothing effect, especially on the sharp tongues of instability, and delay the onset, as shown by Benjamin & Ursell (1954) and Ciliberto & Gollub (1985). Surface tension on the other hand will slightly modify the resonant frequencies. It is important to note that the electromagnetic force, and hence the velocity field, is rotational in the presence of non-axisymmetric modes, so viscous dissipation occurs in the body of the flow. Nevertheless, the Reynolds number based on the frequency and wavelength L_1 of the $m = 1$ mode, namely

$$Re = \omega L_1^2/\nu,$$

is generally very large in the quoted experiments, and such viscous effects must be negligible. As noted by Benjamin & Ursell (1954) viscosity plays a more important role in the sidewall boundary layers. An estimate of the ratio between the pressure variations due to gravity and the viscous wall friction τ may be obtained as follows. The boundary-layer thickness δ and viscous stress τ are given by

$$\delta = (\nu/\omega)^{\frac{1}{2}}, \quad \tau = \rho\nu\omega\eta/\delta.$$

Using typical values for mercury, $\omega = 10\ \mathrm{s}^{-1}$, $\rho = 1.36 \times 10^4\ \mathrm{kg\ m}^{-3}$, $\nu = 10^{-7}\ \mathrm{m}^2\ \mathrm{s}^{-1}$, the value of the ratio of wall friction to hydrostatic pressure, $\tau/\rho g\eta = 10^{-2}$. Thus it appears that viscosity is still negligible except for the highest frequencies. As regards surface tension, its effect becomes non-negligible as soon as the characteristic lengthscales of the free surface are less than the typical length $(\gamma/\rho g)^{\frac{1}{2}}$. Even in mercury this lengthscale is very small – approximately 2 mm.

Throughout this analysis we have neglected the steady velocity field arising from the mean component of the Lorentz force. Numerical calculations performed by GF using a k–ϵ turbulence model, indicate that $\bar{u}/V_A = O(10^{-2})$, where $\bar{u}$ is a typical mean

ω_{GF}(rad/s)	m	m'	Ω_m	$\frac{\lvert\Omega_m-\omega_{GF}\rvert}{\Omega_m}$	L_0	L_0'
21.15	3	3	20.32	1.1×10^{-2}	0.17	0.14
25.32	5	5	25.88	2.2×10^{-2}	0.36	0.24
31.74	8	8	31.73	3.2×10^{-4}	0.003	0.13
37.68	12	12	38.07	1.0×10^{-2}	0.18	0.14
43.96	16	16	43.42	1.3×10^{-2}	0.25	0.14
50.23	22	19	50.33	2.0×10^{-3}	0.047	0.17
56.73	28	22	56.40	6.0×10^{-3}	0.13	0.18
63.08	35	24	62.70	6.0×10^{-3}	0.14	0.21

TABLE 2. Comparison of experimental and theoretical mode excitation. The primes indicate experimentally measured parameters.

flow speed, and V_A the Alfvén speed. For a magnetic field strength of 0.2 T, this means that $\bar{u}/a\omega S \approx 5\times10^{-2}$, so the mean flow is much weaker than that associated with axisymmetric waves – i.e. with the velocity field v_0. Our neglect of the mean flow therefore seems justified for the GF experimental parameters.

Despite the difficulties in making precise comparisons with experiment, it seems likely that the parametric instability corresponds to the transition between regimes II (waves of frequency 2ω) and III (non-axisymmetric waves excited by subharmonic transitions) observed by GF. As predicted, the growth of non-axisymmetric modes occurs only when the field strength exceeds a critical value, and the observed dominant mode number m depends on the applied frequency. In theory the mode number m to be first excited will be that for which the threshold L_0 is smallest – roughly speaking that mode which has a resonant frequency closest to the applied frequency. In practice however the situation is more complicated. The resonance points $k \geqslant 2$ represent weak transitions with growth rates $O(L_0^2)$, and for the GF experiments L_0 was of order 10^{-1}. Such weak growth is easily damped by viscosity and in practice the observed mode is likely to be the one whose fundamental resonance Ω_1 is closest to ω.

Table 2 compares a number of GF observations with theory. For various experimental frequencies ω_{GF} the observed mode number m is compared with m' – the mode which has Ω_1 closest to ω_{GF}. The suggestion of the previous paragraph is supported except for the very high-m modes, which may be significantly affected by surface tension. Even for small-m modes (e.g. $m = 3$) which are influenced by v_0, the mode number predictions are accurate. This is not surprising since our argument simply singles out the mode which responds most readily at the given applied frequency, irrespective of the details of the forcing mechanism.

It can be shown (Nayfeh & Mook 1979) that in the vicinity of the dominant resonance $\omega = \Omega_1$ the stability boundary can be approximated by the pair of straight lines

$$L_0 = \frac{4|\omega-\Omega_1|}{C_{11}\Omega_1}.$$

This formula can be used to make a simple comparison of the observed threshold L_0' with the theoretical value, $L_0 = 4|\omega_{GF}-\Omega_1|/C_{11}\Omega_1$. Here the agreement is not so precise – for a number of reasons.

Most importantly, only small values of L_0 (or order 10^{-1}) could be attained experimentally, so all observed transitions were at applied frequencies close to Ω_1.

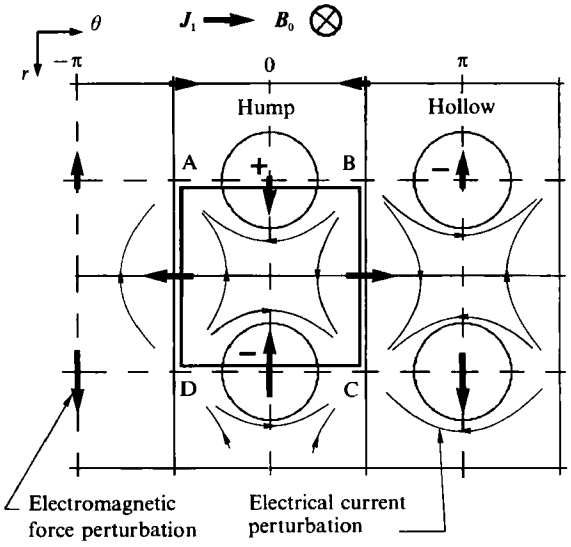

FIGURE 4. Physical illustration of the instability mechanism.

Slight inaccuracies in the experimental parameters could cause a much larger relative error in the frequency separation $|\Omega_1-\omega|$, and hence in the theoretical estimate of L_0. In particular the Perspex tank deformed slightly under the weight of mercury and it proved difficult to measure the radius a to within an accuracy of more than 1 mm. Such a variation in a could cause a change in the theoretical L_0 of as much as 50%! Table 2 shows that the least accurate predictions of L_0 occur when the relative frequency separation is small, in which case the experimental L_0 is somewhat larger since damping will round-off the sharp point of the instability boundary where it meets the axis.

In practice it proved difficult to measure the threshold L_0. The transition exhibited some hysteresis – i.e. the critical L_0 for appearance of non-axisymmetric waves as the current increased, was somewhat larger than the L_0 at which they disappeared as the current decreased – indicating that nonlinear effects are not entirely negligible.

4.3. *Physical interpretation*

It is of interest to examine the physical mechanism underlying the parametric instability. The main cause of the non-axisymmetric mode is the perturbation in the initial purely azimuthal current $\boldsymbol{J}$ due to the free-surface deformation. This perturbation interacts with the applied magnetic field to create Lorentz force perturbations which must be balanced by pressure and inertial forces. We consider for example a control volume bounded by the contour ABCD (figure 4) and the radial force balance. The radial growth of the electric current $\boldsymbol{J}$ leads to a radial increase in the electromagnetic force perturbation. Assuming a balance between pressure and the electromagnetic forces (this holds for example near the lateral wall) we find

$$p(R)-p(Q) = \int_{QR} \nabla p \cdot \mathrm{d}\boldsymbol{x} = \int_{QR} F_r \,\mathrm{d}r < 0,$$

where Q and R are points on AB and CD respectively. This shows that the pressure must be greater on AB than CD, and consequently the liquid metal height must be greater on AB than CD. The present mechanism illustrates how the electromagnetic force perturbations can reinforce the free-surface deformation.

The radial dependence of J appears to be essential. We have carried out similar calculations for an infinitely long two-dimensional tank, in which J is constant and directed along the tank. An equation similar to (2.28a) is obtained, but the diagonal coefficients C_{tt} all vanish, so the most important resonance is absent.

5. Conclusions

According to our theory the effect of a low-frequency alternating magnetic field on a cylindrical tank of liquid metal is twofold: (i) forced axisymmetric ($m = 0$) standing waves are established, and (ii) non-axisymmetric modes ($m \geqslant 1$) may grow as a result of parametric instability.

The instability of a particular $m \geqslant 1$ mode is governed by a system of coupled Mathieu-type equations for the Fourier–Bessel expansion coefficients. Instability occurs when ω and L_0 (forcing frequency and non-dimensional magnetic field strength) lie in certain regions of the parameter plane. The geometry of the instability regions is complicated because of the infinite set of resonant frequencies, which are rational combinations of the natural frequencies. However, the strongest instability represents subharmonic transition to a mode of frequency ω – half the frequency of the basic Lorentz force.

The theory agrees at least qualitatively with experiment, in that the appearance of non-axisymmetric modes occurs at a threshold magnetic field intensity. Observed spectra generally show dominant subharmonic modes, and the mode number m most susceptible to excitation is accurately predicted.

A. D. S. gratefully acknowledges support from the Institut National Polytechnique de Grenoble for two visits, each of two months duration, to MADYLAM. Much of this work was carried out during these visits.

Appendix

Equations (2.19), (2.23), and the standard formulae for Fourier series, give

$$\gamma_{np}^{(1)} = \frac{2R}{R^2\zeta_n^2 + p^2\pi^2} \quad (p \geqslant 0), \qquad \gamma_{n0}^{(1)} = \frac{1}{R\zeta_n^2}, \tag{A 1}$$

where $R = h/a$ is the aspect ratio of the cylinder, and $\zeta_n = \lambda_n a$ is the nth zero of J'_m.

From (2.26) and (2.27)

$$\gamma_{pq}^{(2)} = \langle \psi_p, \phi_q \rangle / \|\phi_q\|^2,$$

where the inner product operator is defined by

$$\langle f, g \rangle = \int_0^a r f(r)\, g(r)\, \mathrm{d}r \quad \text{and} \quad \|f\|^2 = \langle f, f \rangle.$$

Equations (2.19) and (2.24) show that ϕ_q and ψ_p satisfy the following equations and boundary conditions:

$$r^2\phi'' + r\phi' + (\lambda_q^2 r^2 - m^2)\,\phi_q = 0; \quad \phi_q(a) = 1; \quad \phi'_q(a) = 0; \tag{A 2a–c}$$

$$r^2\psi''_p + r\psi'_p - (\mu_p^2 r^2 + m^2)\,\psi_p = 0; \quad \psi'_p(a) = 1/a. \tag{A 3a, b}$$

Multiplying (A 2) by $2\phi'_q$ gives

$$\mathrm{d}/\mathrm{d}r\,(r\phi'_q)^2 + (\lambda_q^2 r^2 - m^2)\,\mathrm{d}/\mathrm{d}r\,(\phi_q^2) = 0.$$

Integrating from $r = 0$ to $r = a$ and using the boundary values (A 2b, c) gives

$$\|\phi_q\|^2 = \tfrac{1}{2}(a^2 - m^2/\lambda_q^2). \tag{A 4}$$

Now multiplying (A 2) by ψ_p, (A 3) by ϕ_q, and subtracting, yields

$$(rw)' + (\lambda_q^2 + \mu_p^2)\,\phi_q \psi_p r = 0; \quad w = \phi_q' \psi_p - \phi_q \psi_p'.$$

Integrating from $r = 0$ to $r = a$, we find

$$\langle \phi_q, \psi_p \rangle = 1/(\lambda_q^2 + \mu_p^2),$$

and (A 4) gives

$$\gamma_{pq}^{(2)} = \frac{2\zeta_q R^2}{(\zeta_q^2 R^2 + p^2\pi^2)(\zeta_p^2 - m^2)}. \tag{A 5}$$

From (2.28b), (A 1) and (A 5) it follows that

$$C_{nk} = \frac{2m^2 R^3 \zeta_n^2}{\zeta_n^2 - m^2} \sum_{p=-\infty}^{\infty} \frac{1}{(R^2\zeta_k^2 + p^2\pi^2)(R^2\zeta_n^2 + p^2\pi^2)},$$

and using the summation formulae,

$$\sum_{p=-\infty}^{\infty} \frac{1}{(a^2 + p^2\pi^2)(b^2 + p^2\pi^2)} = \frac{1}{b^2 - a^2}\left(\frac{1}{a\tanh a} - \frac{1}{b\tanh b}\right),$$

$$\sum_{p=-\infty}^{\infty} \frac{1}{(a^2 + p^2\pi^2)^2} = \frac{1}{2a^3\tanh a} + \frac{1}{2a^2\sinh^2 a},$$

and (A 1) and (A 5), we obtain finally,

$$C_{nk} = \frac{2m^2\zeta_n^2}{(\zeta_n^2 - m^2)(\zeta_n^2 - \zeta_k^2)}\left(\frac{1}{\zeta_k \tanh(R\zeta_k)} - \frac{1}{\zeta_n \tanh(R\zeta_n)}\right) \quad (k \neq n), \tag{A 6a}$$

$$C_{kk} = \frac{m^2}{\zeta_k - m^2}\left(\frac{1}{\zeta_k \tanh(R\zeta_k)} + \frac{R}{\sinh^2(R\zeta_k)}\right). \tag{A 6b}$$

Since $\zeta_1 > m$ the coefficients are all positive. In the limit $m \to \infty$, $\zeta_1 \approx m + 0.80862m^{\frac{1}{3}}$ (Abramowitz & Stegun 1965, formula 9.5.16) and one can derive the asymptotic formula,

$$C_{11} \approx 0.61834m^{-\frac{1}{3}} \quad \text{as} \quad m \to \infty.$$

REFERENCES

Abramowitz, M. & Stegun, I. E. 1965 *Handbook of Mathematical Functions*. Dover.

Arnol'd, V. I. 1973 *Ordinary Differential equations*. MIT Press.

Benjamin, T. B. & Ursell, F. 1954 The stability of a plane free surface of a liquid in vertical periodic motion. *Proc. R. Soc. Lond.* A **225**, 505–515.

Briskman, V. A. & Shaidurov, G. F. 1968 Parametric instability of a fluid surface in an alternating electric field. *Sov. Phys. Dokl.* **13**, 540–542.

Ciliberto, S. & Gollub, J. P. 1985 Chaotic mode competition in parametrically forced surface waves. *J. Fluid Mech.* **158**, 381–398.

Davidson, P. A., Hunt, J. C. R. & Moros, A. 1988 Turbulent recirculating flows in liquid metal MHD. Proc. 5th Beer-Sheva Seminar on MHD flows and turbulence. In *Liquid Metal Flow: Magnetohydrodynamics and Applications* (ed. H. Branover, M. Mond & Y. Unger). Prog. in Astron. and Aeron., vol. 111, pp. 400–420. AIAA.

Faraday, M. 1831 On the forms and states assumed by fluids in contact with vibrating elastic surfaces. *Phil. Trans. R. Soc. Lond.* **121**, 319–340.

FAUTRELLE, Y. R. 1981 Analytical and numerical aspects of the electromagnetic stirring induced by alternating magnetic fields. *J. Fluid Mech.* **102**, 405–430.

GALPIN, J. M. & FAUTRELLE, Y. 1992 Liquid-metal flows induced by low-frequency alternating magnetic fields. *J. Fluid Mech.* **239**, 383–408 (referred to herein as GF).

GEL'FAND, I. M. & LIDSKII, V. B. 1958 On the structure of the regions of stability of linear canonical systems of differential equations. *Am. Math. Soc. Transl.* **8** (2), 143–182.

JORDAN, D. W. & SMITH, P. 1987 *Nonlinear Ordinary Differential Equations*. Oxford University Press.

MIKELSON, Y. Y., JAKOVITCH, A. T. & PAVLOV, S. I. 1978 Numerical investigation of averaged MHD flow in cylindrical regions with the adoption of working hypotheses for turbulent stresses. *Magnit. Girodin.* **14**, 51–58.

MILES, J. W. 1984 Resonantly forced surface waves in a circular cylinder. *J. Fluid Mech.* **149**, 15–31.

MILES, J. W. & HENDERSON, D. 1990 Parametrically forced surface waves. *Ann. Rev. Fluid Mech.* **22**, 143–165.

MOFFATT, H. K. 1984 High frequency excitation of liquid metal systems. In *Proc. IUTAM Symp. on Metallurgical Applications of MHD, 1982, Cambridge UK*, pp. 180–189. London: The Metals Society.

MOORE, D. J. & HUNT, J. C. R. 1984 Flow, turbulence and unsteadiness in coreless induction furnaces. In *Proc. IUTAM Symp. on Metallurgical Applications of MHD, 1982, Cambridge UK*, pp. 93–107. London: The Metals Society.

NAYFEH, A. H. & MOOK, D. T. 1979 *Nonlinear Oscillations*. Wiley.

SNEYD, A. 1971 Generation of fluid motion in a circular cylinder by an unsteady applied magnetic field. *J. Fluid Mech.* **49**, 817–827.

SNEYD, A. 1979 Fluid flow induced by a rapidly alternating or rotating magnetic field. *J. Fluid Mech.* **92**, 35–51.

TABERLET, E. & FAUTRELLE, Y. 1985 Turbulent stirring in an experimental induction furnace. *J. Fluid Mech.* **159**, 409–431.

TARAPORE, E. & EVANS, J. W. 1976 Fluid velocities in induction melting furnaces, part 1: theory and laboratory experiments. *Metall. Trans.* B **7**, 343–351.

TRAKAS, C., TABELING, P. & CHABRERIE, J. P. 1984 Etude expérimentale du brassage turbulent dans le four à induction. *J. Mec. Theor. Appl.* **3**, 345–370.